Enhancing Vibration Signal Measurement Accuracy in Machine Tool Bearings Using Multi-Sensor Data Fusion Techniques

Word Count: 4017

Abstract

This research aims to enhance the accuracy of vibration signal measurement in machine tool bearings under complex conditions by utilizing multi-sensor data fusion techniques. Single-sensor monitoring often struggles with environmental noise and synchronization issues. To address this, a dual-platform data acquisition system was developed using STM32 microcontrollers and FPGA hardware, with the FPGA offering improved sampling rate and synchronization (Liao et al., 2023).

Three ADXL345 accelerometers were mounted around the x -axis bearing of a VM1050S CNC machine to collect tri-axial vibration data (Holovatyy et al., 2017). The exponentially weighted moving average (EWMA) method was used to preprocess data and reduce jitter. For fusion, three algorithms were tested — Kalman filter, particle filter, and Dempster–Shafer (D-S) evidence theory. D-S theory was selected due to its superior handling of uncertainty without requiring prior probabilistic models (Liang et al., 2022). Experimental results showed that FPGA-based D-S fusion achieved a mean squared error (MSE) of 0.00252, closely matching Siemens benchmark data while maintaining lower cost. These findings highlight the effectiveness of combining FPGA architecture with D-S evidence theory for accurate, low-cost vibration monitoring, with potential for broader use in intelligent fault diagnosis systems.

Keywords： Multi-sensor data fusion, vibration signal, machine tool bearing, STM32, FPGA, Kalman filter

Enhancing Vibration Signal Measurement Accuracy in Machine Tool Bearings Using Multi-Sensor Data Fusion Techniques

This research project began in the summer following the completion of my AP Seminar course, prior to the formal start of AP Research. Motivated by my initial interest in engineering and embedded systems, I started exploring the accuracy limitations of single-sensor vibration monitoring in complex machine environments.

After building the initial data acquisition prototype, I completed the first full draft of the research paper in the months following summer break. As my investigation deepened — particularly in sensor fusion theory and data synchronization — I revisited and improved aspects of the original system design, including replacing the STM32-only setup with an FPGA-based parallel acquisition platform for enhanced precision and timing.

Vibration detection plays a crucial role in fields such as equipment maintenance, structural integrity assessment, and environmental monitoring. Acceleration sensors are capable of converting mechanical vibrations into electrical signals, facilitating easier processing and analysis. However, as application environments become increasingly complex, the accuracy and reliability provided by a single sensor are often insufficient. As a result, multi-sensor data fusion technology has garnered significant attention for its ability to enhance the reliability and robustness of measurement outcomes.

This research utilizes the ADXL345 accelerometer, which can measure vibration acceleration across three axes. Three identical accelerometers were installed at

different positions on the bearings of a VM1050S model CNC machine tool to independently collect vibration acceleration signals. Initially, data acquisition was conducted using an STM32 microcontroller; however, due to its single-threaded architecture, synchronization among sensors was suboptimal. Subsequently, an FPGA-based system was developed, leveraging its high parallel processing capability to achieve a high-precision, high-synchronization multi-sensor data acquisition system, thereby improving overall measurement accuracy. Additionally, the exponentially weighted moving average method was applied to preprocess the collected signals, minimizing data jitter. After evaluating various data fusion algorithms, including Kalman filtering, particle filtering, and D-S evidence theory, D-S evidence theory was ultimately selected for fusion experiments.

This project seeks to answer the **research question: How Can Multi-Sensor Fusion Methods Improve Signal Accuracy and Reliability in Complex Environments?** By comparing the fused results with those from a Siemens vibration testing system, the final experimental outcomes demonstrated that the data fusion approach significantly enhanced the measurement accuracy of vibration acceleration signals, offering solid theoretical support and promising applications for research in equipment fault diagnosis and related fields.

Data Collection System

Vibration Acceleration Sensor

The accuracy of the collected data directly affects data analysis results. This research used the ADXL345 accelerometer for data collection. ADXL345 is a

high-precision, ultra-low power consumption, digital output three-axis accelerometer developed by Analog Devices (Holovatyy et al., 2017). The accelerometer offers measurement ranges of $\pm 2g$, ± 4g , ± 8g and $\pm 16g$, it can not only measure acceleration caused by vibration but also acceleration at rest. It contains a mechanical device inside that can sense motion (Apriyansa et al., 2021). This component is very sensitive to external force changes, much more sensitive than ordinary solid-state electronic products.

A three-axis accelerometer can detect vibration acceleration on three axes simultaneously, as shown in Figure 1 When the chip is placed in the same direction as in the figure, the acceleration on the x -axis and y -axis is $0g$, and the acceleration on the z-axis is $+1$g (g is the earth's gravity acceleration). When the chip direction is opposite, the acceleration values on the x -axis and y -axis remain unchanged, and the acceleration value on the z-axis is -1g.

Figure 1

Three Axial Components of ADXL345

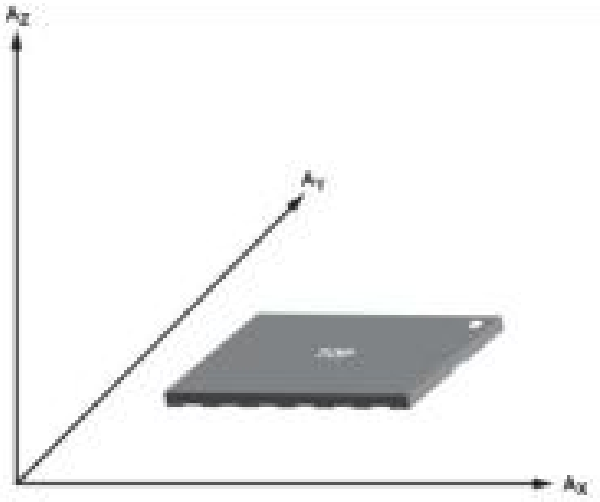

In the first two cases, no vibration acceleration will be detected on the x and y axes. When the ADXL345 is placed vertically and rotated 90° clockwise three times, the rotation results are shown in Figure 2. In these four cases, the acceleration value of the two axes is $0g$ each time.

In the actual vibration detection process, ADXL345 is usually fixed on the rotating mechanical equipment. When the vibration is large, vibration components are detected in each axis, but the vibration components in the axial direction are smaller and the vibration components in other directions are larger.

Figure 2

ADXL345 Acceleration Value Under Special Circumstances

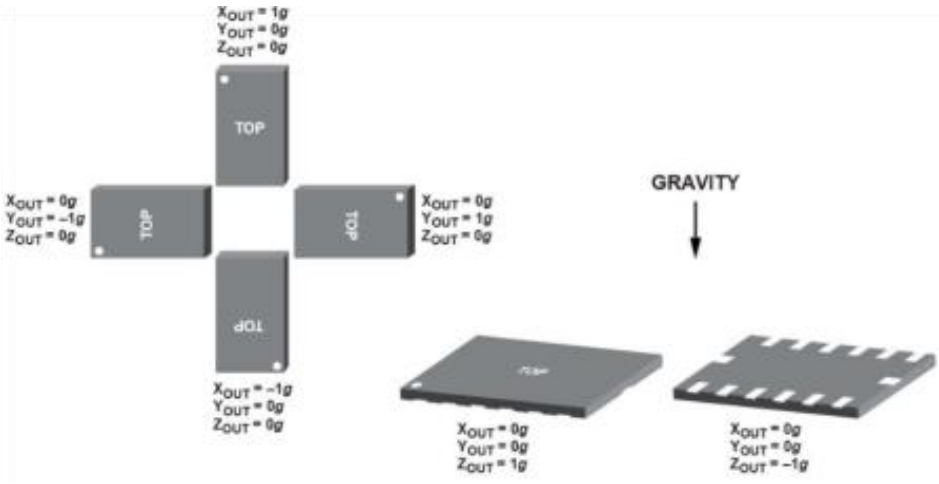

The circuit design schematic diagram of the ADXL345 module is shown in Figure 3. Commonly used data transmission interfaces are SPI (3-wire or 4-wire) and I2C, and the data format is 16-bit two's complement. The CS pin is pulled up to VDD I/O, enabling I2C mode. Due to the limitation of the communication speed, when using 400kHz I2C, the maximum output data rate is 800Hz; in SPI mode, the CS pin is controlled by the bus master. When using an SPI bus over 2MHz, the output speed can be selected from 3200Hz and 1600Hz.

Figure 3

ADXL345 Schematic Diagram

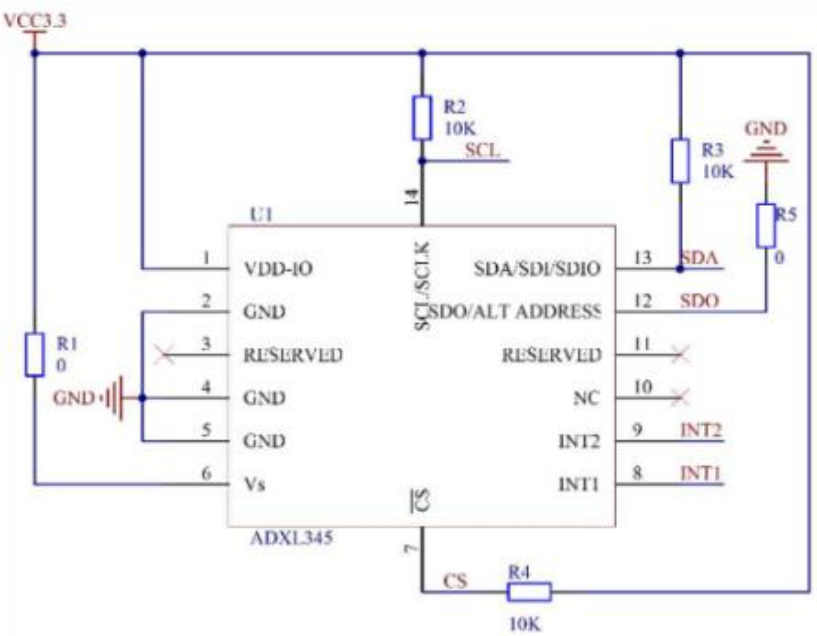

Collection System Construction

Data Collection Solution Based on STM32

The data acquisition system mainly constitutes a power supply unit, a microcontroller unit, a serial communication unit, a multi-channel analog-to-digital converter unit, and a sampling channel interface unit. Figure 4 shows the microcontroller unit. Its model is STM32F103C8T6. It is a 32-bit microcontroller based on the Cortex-M3 core launched by Italian and French Semiconductor Company (ST). The hardware is packaged in LQFP48 and belongs to the ST. STM32 series in microcontrollers (Liao et al., 2023).

Figure 4

Microcontroller Unit Circuit Schematic Diagram

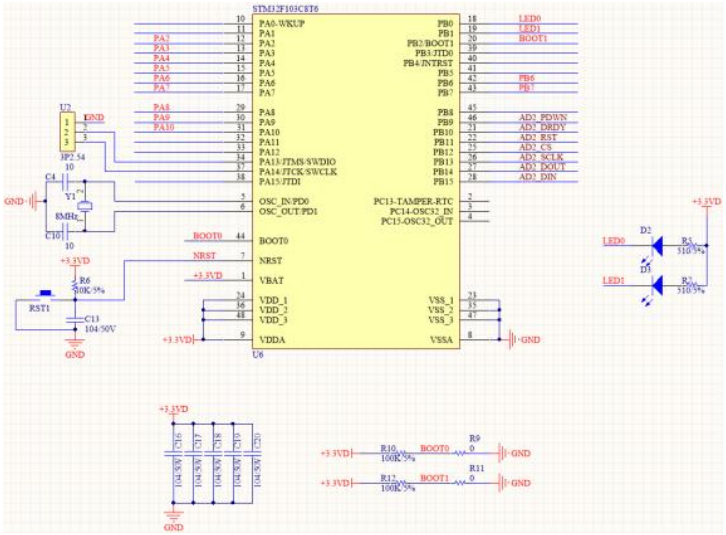

Note. STM32F103C8T6 is a model in the STM32 series of MCUs. It has rich resources. Its core is Cortex-M3, with a main frequency of up to 72MHz, internal storage Flash size of 64KB, SRAM size of 20KB, 37 IO ports, and 4 timings. device and 3 UARTs, etc. The details are shown in Table 1.

Table 1

STM32F103C8T6 Internal Resource Table

STM32F103C8T6 RESOURCES		STM32F103C8T6 RESOURCES	
Core	Basic Timers	Core	Cortex-M3
Frequency	General Timers	Frequency	72MHz
Flash	Advanced Timer	Flash	64KB
64KB	12-bit ADC	SRAM	20KB
20KB	ADC Channels	Package	37
Package	RTC 1	Opering Voltage	37
I/O Pins	USART/UART 3	Basic Timers	0
Supply Voltage	CAN 3	General Timers	3
App to Voltage	SPI 2	Advanced Timers	1
2.4V-3.6V	I2C 2	12-bit ADC	1
USB Device	DMA Device 1	ADC Channels	18
		RTC	USART/UART
		I/W W DG	CAN
		SPI	2
		IIC	2

Figure 5 below shows the multi-channel analog-to-digital converter unit. The model selected for the analog-to-digital converter is ADS1256, which is a micro-power consumption, high-precision, 8-channel, and 24-bit high-performance analog model launched by Texas Instruments (TI) digital converter (ADC). This device offers up to 23-bit noise-free accuracy, data rates up to 30kSPS (subsamples/second), 0.0010% nonlinearity (max),numerous on-board peripherals (input analog multiplexers, input buffers, Programmable gain amplifier and programmable digital filter, etc.), and can provide designers with a complete and high-resolution measurement solution.

Figure 5

Multi-Channel Analog-to-Digital Converter

Unit Circuit Schematic Diagram

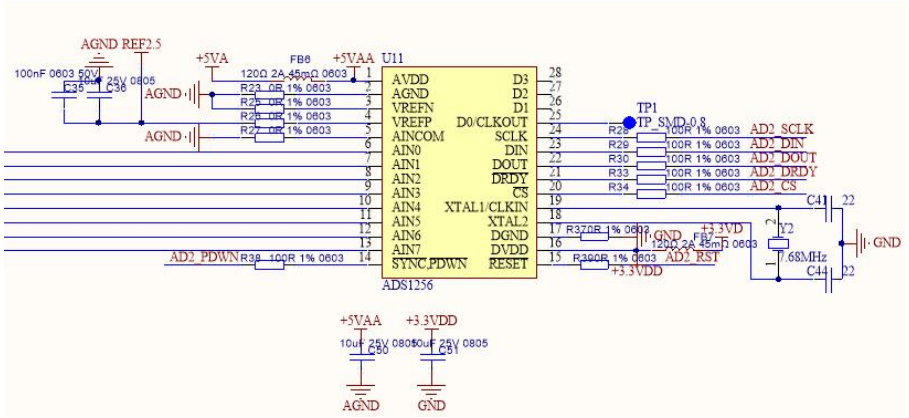

Figure 6 below shows the power supply unit. Power supply is the input through

the +5V power supply, which is converted to +3.3V through the ADP3338 chip to power the microcontroller. At the same time, the +5V input is connected through magnetic beads to the +5VA ouput for the analog part of the analog-to-digital converter. Power supply, digital ground, and analog ground are separated by 0 ohm resistors. All voltage outputs are filtered by capacitors to reduce power supply voltage fluctuations and filter noise such as harmonics.

Figure 6

Schematic Diagram of the Power Supply Unit Circuit

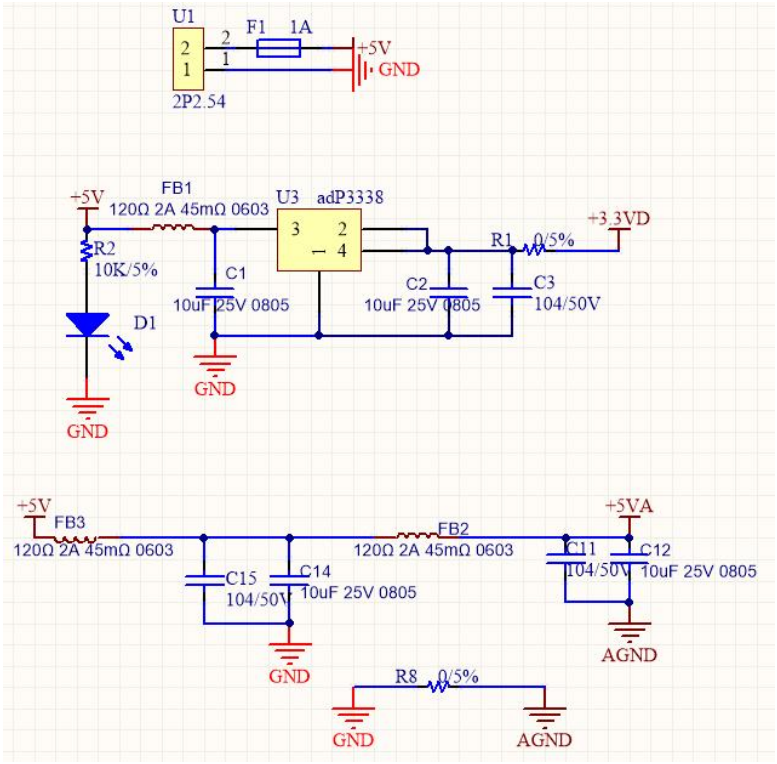

Figure 7 below shows the sampling interface unit, which uses a multi-channel connector as the external sampling channel interface to connect the acceleration sensor for detecting vibration signals. Meanwhile, it performs low-pass filtering on

the input signal to reduce signal noise and external interference and improve signal quality.

Figure 7

Sampling Interface Unit Circuit Schematic Diagram

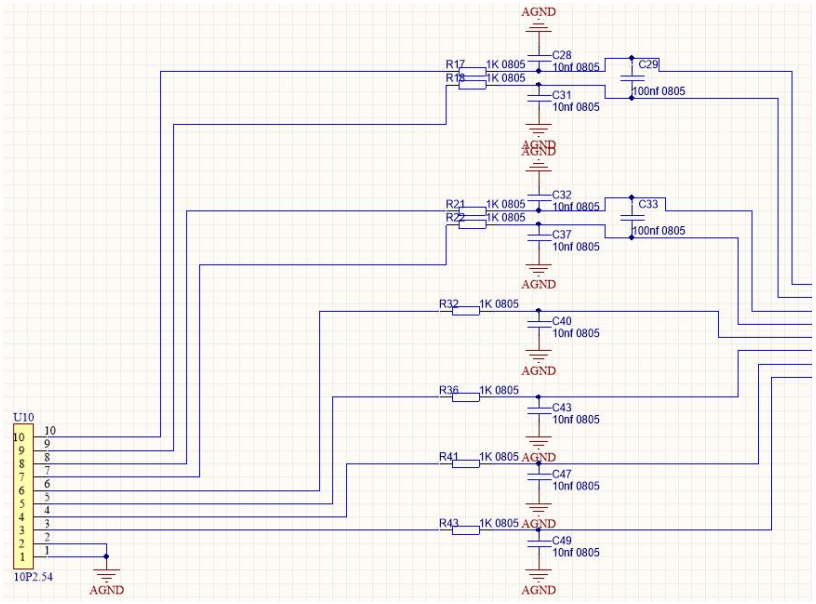

Figure 8 below shows the serial communication unit, which uses the RS232 communication interface to communicate with the host computer and transmits the collected data to the host computer for storage and data analysis.

Figure 8

Serial Communication Unit Circuit Schematic Diagram

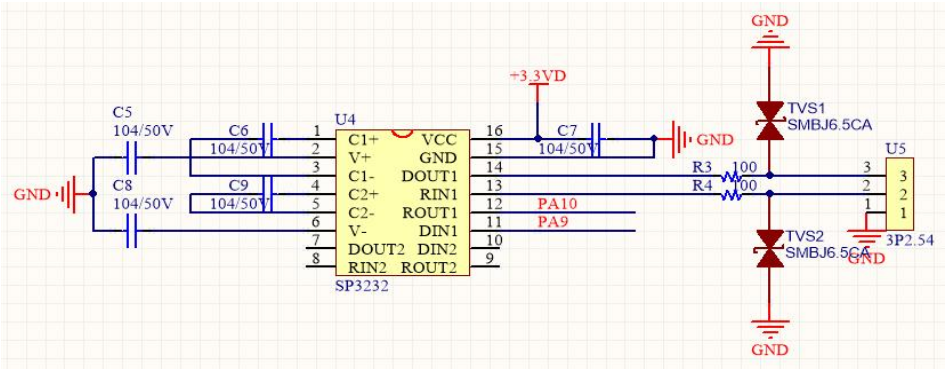

The PCB design diagram is shown in Figure 9. It adopts a two-layer board design to separate the digital circuit part and the analog circuit part, and lays copper on the two parts with different grounds, which greatly reduces interference and noise and improves the performance of the board. The physical picture of the final welding and debugging is shown in Figure 10.

Figure 9

PCB Board Layout Design Drawing

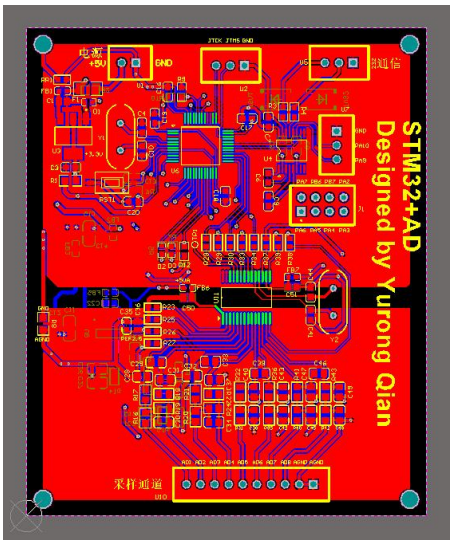

Figure 10

Physical Diagram of Circuit

FPGA-based Data Acquisition Solution

In order to further enhance the real-time capabilities of multi-channel data sampling, increase the circuit system's sampling rate, and expand the number of available sampling channels, it was necessary to develop a controller with parallel processing capabilities to build a higher-performance circuit system. To accomplish this objective, a multi-channel data acquisition system utilizing field programmable gate array (FPGA) chips was designed. FPGA (Field Programmable Gate Array) is a programmable logic device that features abundant configurable I/O pins. It is user-friendly, flexible, and supports system-level programmability. FPGA devices are capable not only of implementing traditional combinational logic functions but also of executing complex sequential logic operations. Compared with traditional ASIC (Application Specific Integrated Circuit), FPGA has the characteristics of rich wiring

resources, re-programmability, high integration, and low investment. It has been widely used in the field of digital circuit design, such as communications, computers, consumer electronics, automobiles, etc.

The chip selected for this FPGA-based data acquisition solution is the Cyclone IV series FPGA chip EP4CE6E22C8N from Altera (now acquired by Intel). This chip has 92 IO ports, 6272/10320 logic units, and 2 PLLs. This chip has the characteristics of high performance and high stability, and can well meet our design needs. This data acquisition circuit system consists of a power supply unit, an FPGA controller unit, a multi-channel analog-to-digital converter unit, a serial communication interface, and an external sampling channel interface.

Figure 11 shows the circuit schematic diagram of the FPGA controller unit of this circuit system. The multi-channel analog-to-digital converter unit, power supply unit, sampling interface, and serial communication interface are shown in Figures 5, 6, 7 and 8 respectively, and will not be described here again.

Figure 11

FPGA Controller Unit Circuit Schematic Diagram

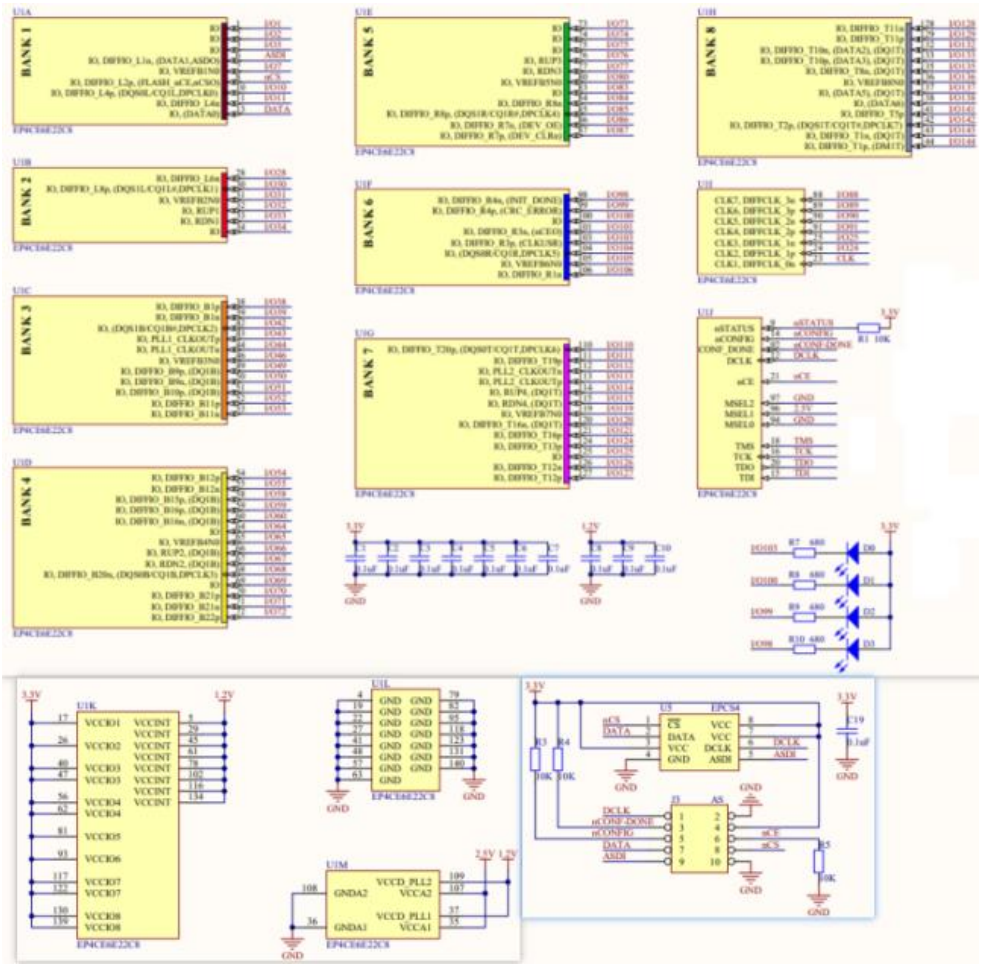

The PCB design diagram is shown in Figure 12. It adopts a two-layer board design to separate the digital circuit part and the analog circuit part, and lays copper on the two parts with different grounds, which greatly reduces interference and noise and improves the performance of the board. The physical picture of the final welding and debugging is shown in Figure 13.

Figure 12

PCB Board Design Drawing

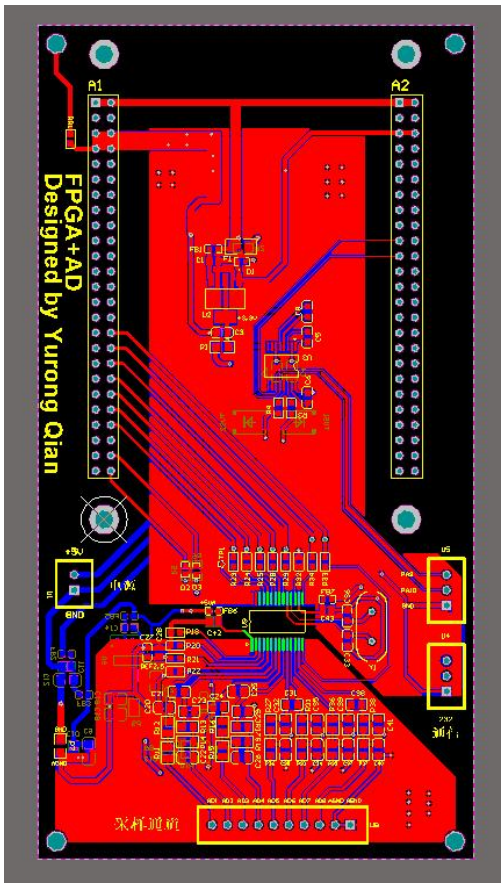

Figure 13

Physical Diagram of Circuit

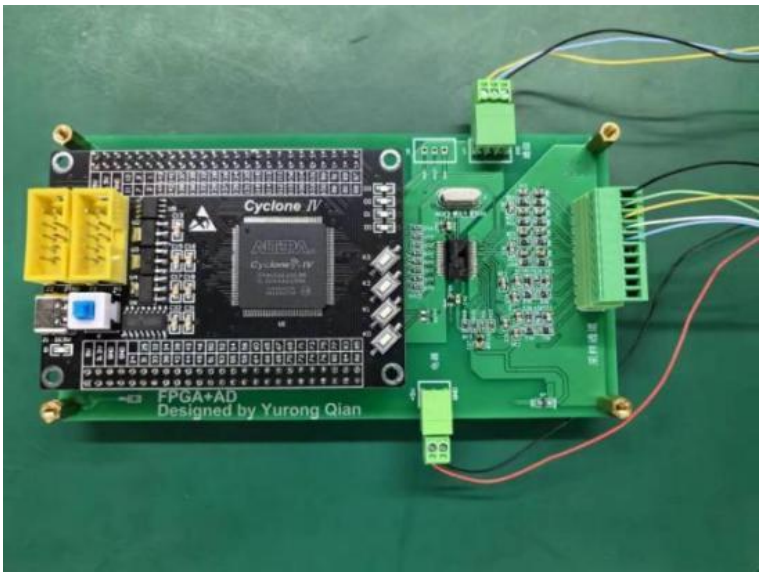

Data Collection

The vertical machining center 1050S model CNC machine tool (shown in Figure 14) was selected to collect bearing vibration data. This model of machine tool has three axes, namely x-axis, y-axis, and z-axis. Each axis can operate independently. A motor is connected to the screw inside each axis to drive the shaft movement. There is a bearing seat at the end of the screw (as shown in Figure 15). The bearing of the x-axis is selected to test its vibration acceleration fluctuations.

Figure 14 & 15

Complete Machine; Bearing Seat

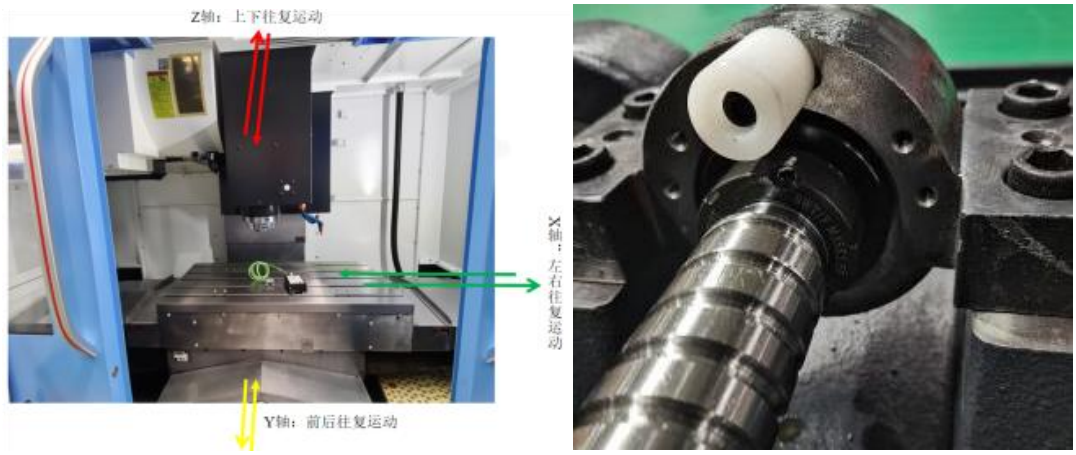

Among them, the internal structure of the x-axis is shown in Figure 16.

Figure 16

x-axis Internal Structure Diagram

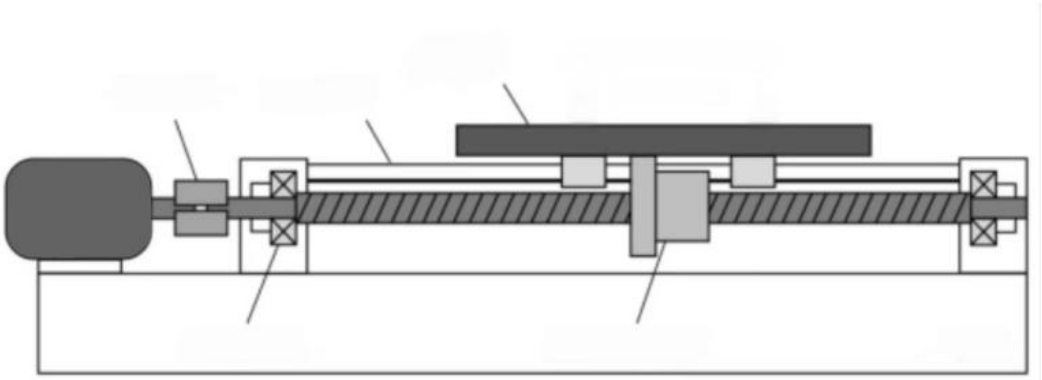

Here, three identical vibration acceleration sensors are used, which are installed around the bearings at 60° intervals (as shown in Figure 17 below). At the same time, the vibration data of each position when the CNC machine runs is measured. During each test, the running action of the machine tool must be ensured to be consistent. When the bearing running speed is stable, it starts collecting data from three sensors.

Figure 17

Data Collection Process

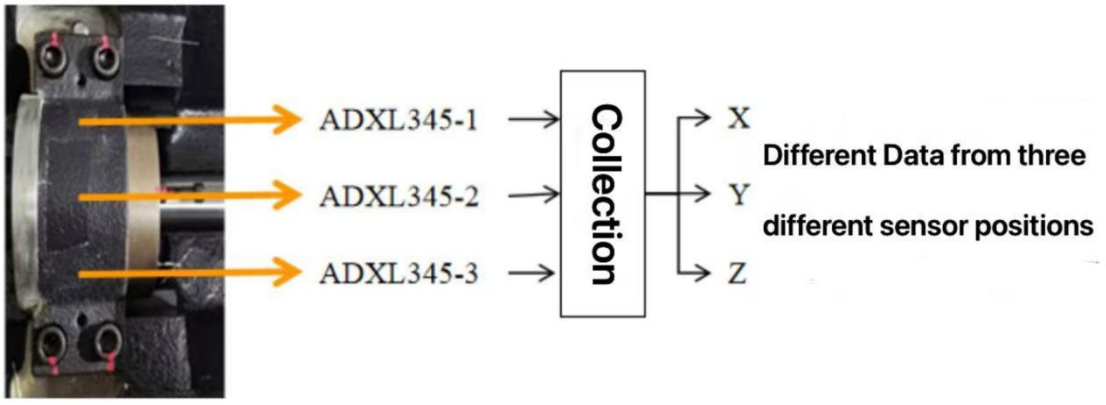

Figure 18 below shows when the rotation speed at the bearing is stable at 3000r/min. The three vibration acceleration sensors at different positions

simultaneously collect data waveforms in the X direction when the x -axis of the machine tool runs. It can be seen that when the same sensor is placed at different locations, there are differences in the data collected, so subsequent data fusion should be performed to more comprehensively represent the true situation of the bearing operation.

Figure 18

Multi-Sensor Data Waveform Diagram

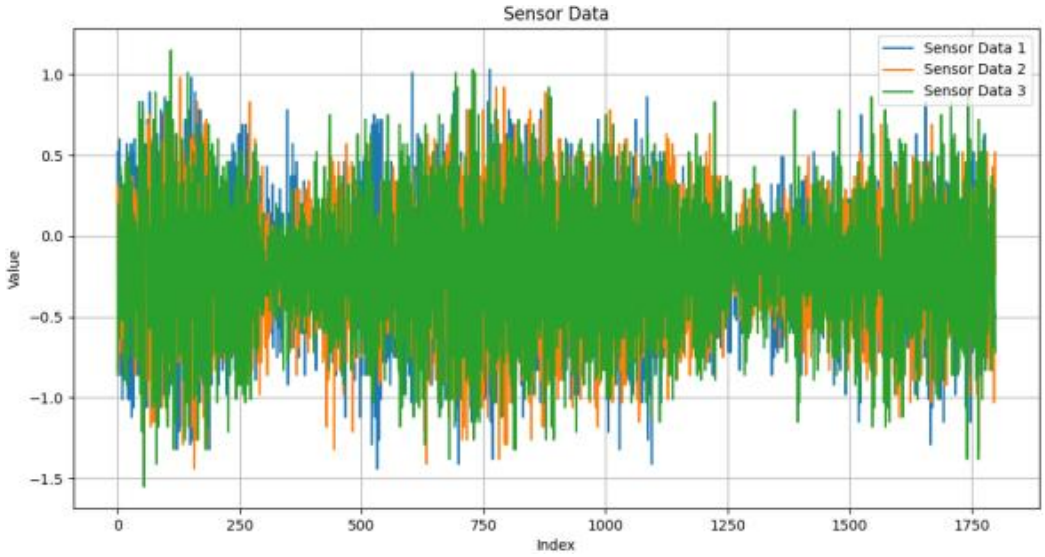

Data Fusion Method

At the data fusion level, we study some common data fusion methods, including Kalman filter, particle filter, D-S evidence theory, etc.

Kalman Filter

Kalman filter is a recursive algorithm for linear system state estimation and is widely used in signal processing, control systems, navigation, and other fields. It

obtains the optimal estimate by minimizing the mean square error of the estimation error. The basic idea is to use the state space model of the system, combined with measurement data, to optimally estimate the system state through recursion (Zhou et al., 2020). It consists of two main steps: prediction and updating.

System model: state transition equation (Equation 3.1) and observation equation (Equation 3.2):

$$x_k = A_{k-1}x_{k-1} + B_{k-1}u_{k-1} + \omega_{k-1} \tag{3.1}$$

$$z_k = H_k x_k + v_k \tag{3.2}$$

Among them, x_k is the state vector of the system at time k, u_{k-1} is the control vector, z_k is the observation vector, A_{k-1} is the state transition matrix, B_{k-1} is the control matrix, H_k is the observation matrix, and ω_{k-1} and v_k are the process noise and observation noise respectively.

(1) Prediction steps: state prediction (Equation 3.3) and error covariance prediction (Equation 3.4)

$$\hat{x}_{k|k-1} = A_{k-1}\hat{x}_{k-1|k-1} + B_{k-1}u_{k-1} \tag{3.3}$$

$$P_{k|k-1} = A_{k-1}P_{k-1|k-1}A_{k-1}^T + Q_{k-1} \tag{3.4}$$

(2) Update steps: Kalman gain (Equation 3.5), state update (Equation 3.6), error covariance update (Equation 3.7)

$$K_k = P_{k|k-1}H_k^T\left(H_k P_{k|k-1}H_k^T + R_k\right)^{-1} \tag{3.5}$$

$$\hat{x}_{k|k} = \hat{x}_{k|k-1} + K_k\left(z_k - H_k\hat{x}_{k|k-1}\right) \tag{3.6}$$

$$P_{k|k} = \left(I - K_k H_k\right)P_{k|k-1} \tag{3.7}$$

Through the above steps, Kalman filtering can recursively update the estimated

value and error covariance of the system state at each moment (Zhu et al., 2023).

Particle Filtering

Particle filtering is a Monte Carlo method for state estimation of nonlinear, non-Gaussian systems (Shen et al., 2023). It estimates the system state by approximating the posterior probability distribution through a large number of random samples (particles). The basic idea is to use a set of weighted particles to represent the probability distribution of the state, make estimates, and update the state through steps such as sampling, importance weighting, and resampling.

Similar to Kalman filter, particle filter is also based on state transition equation (3.8) and observation equation (3.9):

$$x_k = f\left(x_{k-1}, u_{k-1}\right) + \omega_{k-1} \tag{3.8}$$

$$z_k = h\left(x_k\right) + v_k \tag{3.9}$$

Specific steps of particle filtering:

(1) Initialization: Generate N particles $\left\{x_0^{(i)}\right\}_{i=1}^{N}$ and assign initial eights $\omega_0^{(i)} = \frac{1}{N}$.

(2) Prediction: For each particle, perform state prediction according to the state transition equation.

$$x_k^{(i)} \sim p\left(x_k \mid x_{k-1}^{(i)}, u_{k-1}\right) \tag{3.10}$$

(3) Update: Calculate the weight of each particle according to the observation equation.

$$\omega_k^{(i)} \propto \omega_{k-1}^{(i)} p\left(z_k \mid x_k^{(i)}\right) \tag{3.11}$$

(4) Normalized weight: Normalize all weights so that their sum is 1.

$$\omega_k^{(i)} = \frac{w_k^{(i)}}{\sum_{j=1}^{N} w_k^{(j)}} \tag{3.12}$$

(5) Resampling: Resample particles according to their weights to reduce the number of particles with smaller weights and improve the effectiveness of particle representation.

Particle filtering can recursively estimate the system state in nonlinear, non-Gaussian systems (Abdellatif et al., 2023). It is suitable for processing complex dynamic systems. Although the computational complexity is high, it performs well in many practical applications.

D-S Evidence Theory

In real life, the occurrence of most events is uncertain. The so-called rules are based on specific conditions and can only exist in a local space or a short period of time. This is the reason why information or knowledge describing objective phenomena is uncertain. In multi-sensor data fusion, data acquisition and processing are also largely full of uncertainties (Liang et al., 2022). Therefore, solutions to uncertain problems are also important. D-S evidence theory provides great feasibility in this regard.

Identification Frame

For a question that requires a decision, there are many possibilities for the answer. A set $\in$ is the collection of all answers. There are may be both numerical elements and non-numeric elements, and the elements are mutually exclusive. $\in$ is called the identification frame of mutually exclusive events, that is, $\because = \{\theta_1, \theta_2, \cdots, \theta_i, \cdots \theta_N\}$,

where N represents the total number of elements; θ_i is an event in the identification frame.

The power set of $\in$ describe all subsets in the recognition framework, denoted as $2^{\cdot\cdot}$, which is:

$$2^{\cdot\cdot} = \{\varnothing, \{\theta_1\}, \{\theta_2\}, \cdots, \{\theta_N\}, \{\theta_1 \cup \theta_2\}, \{\theta_1 \cup \theta_3\}, \cdots, \cdot\cdot\} \tag{3.13}$$

Among them, $\varnothing$ represents the empty set; $\{\theta_i \cup \theta_j\}$ can also be written as $\{\theta_i, \theta_j\}$, $i, j \in [1, N], i \neq j$.

In the power set $2^{\cdot\cdot}$, elements and answers exist correspondingly, which is evidence. If N elements exist in the recognition frame $\cdot\cdot$, then 2^N elements exist in the power set $2^{\cdot\cdot}$.

Basic Probability Assignment Function (BPA)

Suppose there exists a certain subset A such that $A \subseteq \Theta$, function $m : 2^{\cdot\cdot} \to [0,1]$ satisfies

$$\begin{cases} m(\varnothing) = 0 \\ \sum_{A \subseteq \cdot\cdot} m(A) = 1 \end{cases} \tag{3.14}$$

Then, it can be said that the basic probability distribution function of the recognition frame $\cdot\cdot$ is m. Among them, $m(A)$ is called the basic trust distribution function of event A, which is used to express the trust degree of evidence A.

Trust Function

Suppose there exists a certain subset A and B such that $B \subseteq A \subseteq \cdot\cdot$, B is logically contained in A, and function $Bel : 2^{\cdot\cdot} \to [0,1]$ satisfies

$$Bel(A) = \sum_{B \subseteq A} m(B) \tag{3.15}$$

Then, it can be considered as A's trust function, which is used to express A's trust

degree.

Plausibility Function (Likelihood Function)

Let $Bel : 2^{\because} \to [0,1]$ be a certain trust function on the recognition framework, define $pl : 2^{\because} \to [0,1]$ as the following:

$$\forall A \subset \because, pl(A) = 1 - Bel(\overline{A}) \tag{3.16}$$

Then ^{pl} it is called the plausibility function, which can also be expressed as

$$pl(A) = \sum_{A \cap B \neq \varnothing} m(B) \tag{3.17}$$

The plausibility function is a complement to the trust function and represents the degree of doubt about proposition A.

There is another concept that can assist understanding (Zhu et al., 2021), Jiao Yuan (focal element) : If $m(A) > 0$, then A is called the focal element of the trust function Bel, and the core of the trust function Bel is the union of all focal elements.

D-S Evidence Synthesis Rules

The D-S synthesis rule reflects the interaction between evidence. When the credibility function is synthesized, the synthesized credibility function can become a new credibility function generated after combining the evidence (Ullah et al., 2021). Assume that there are two reliability functions Bel_1 and Bel_2 existing on the recognition framework $\because$, the basic probability distribution functions corresponding to these two reliability functions are m_1 and m_2 , and are used to represent their respective focal elements. Basic probability distribution:

$m_1(A_1), \cdots m_1(A_i), \cdots, m_1(A_k)$ and $m_2(B_1), \cdots m_2(B_j), \cdots, m_2(B_l)$ can be represented by figure 19.

Figure 19

Credibility Distribution of Evidence 1 and Evidence 2

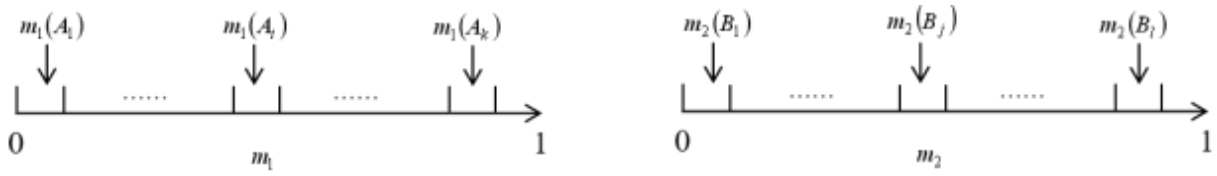

Figure 20

Geometric Interpretation of D-S Evidence Synthesis Rules

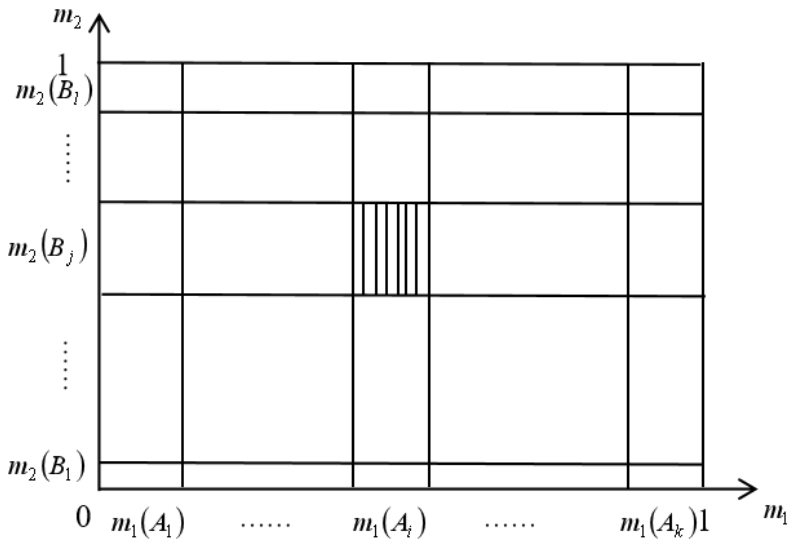

Figure 20 shows the process of jointly considering the two pieces of evidence in Figure 19. Among them, the rectangular area represents the total confidence, the vertical and horizontal lines represent the basic reliability values on focal elements $A_1, A_2, \cdots, A_k$ and $B_1, B_2, \cdots, B_l$ assigned to m_1 and m_2 respectively, and the shaded area stands for the measure $m_1(A_i)m_2(B_j)$, which represents Bel_1 and Bel_2 jointly assigned measure $m_1(A_i)m_2(B_j)$ to $A_i \cap B_j$. When $A \subseteq \because$, if $A_i \cap B_j = A$ exists,

then $\sum_{A_i \cap B_j} = Am_1(A_i)m_2(B_j)$ can be used to represent the total confidence value assigned to A. But if $A_i \cap B_j = \varnothing$, there will be a problem when the reliability $\sum_{A_i \cap B_j} = \varnothing m_1(A_i)m_2(B_j)$ will be assigned to the empty set. The simplest method is to discard the confidence values first and then normalize them. Simply put, each confidence value is multiplied by the coefficient:

$$\frac{1}{1-\sum_{A_i \cap B_j} = \varnothing m_1(A_i)m_2(B_j)} = \frac{1}{1-k} \tag{3.18}$$

Equation (3.18) is called the normalization constant, so

(1) The synthesis rule of two pieces of evidence is:

$$m(A) = \begin{cases} \dfrac{\sum_{A_i \cap B_j} = Am_1(A_i)m_2(B_j)}{1-k}, & A \neq \varnothing \\ 0, \quad A = \varnothing \end{cases} \tag{3.19}$$

(2) The synthesis rule for multiple evidences is:

Assume that n independent evidence bodies are derived from the identification framework $\because$, and record their basic credibility distribution as $m_1, m_2, \cdots, m_n$, then the combination rule can be expressed as:

$$m(A) = \begin{cases} \dfrac{\sum_{A_i \cap B_j} = A\prod_{i=1}^{n} m_1(A_i)}{1-k}, & A \neq \varnothing \\ 0, \quad A = \varnothing \end{cases} \tag{3.20}$$

To sum up, evidence theory is good at dealing with uncertain issues and has been widely used in artificial intelligence, especially multi-sensor data fusion (Deng & Wang, 2020).

Experimental Verification

Data Sources and Preprocessing

The bearing vibration data is collected from the X bearing of the VM1050S

machine tool to keep the x -axis running movements consistent during each test, and the length of the collected data is 1800.

As a non-stationary time series that is related to each other, the bearing vibration signal will bring difficulties to subsequent analysis. The exponentially weighted moving average method (EWMA) can be regarded as a low-pass filter to eliminate short-term fluctuations and retain the long-term development trend, providing a smooth form of vibration signal (Wu et al., 2024). According to the actual observation values, the smoothing process is completed through Equation (4.1):

$$EWMA(t) = \lambda Y(t) + (1-\lambda) EWMA(t-1) \tag{4.1}$$

In the formula: $EWMA(t)$ is the estimated value at the moment t, indicating the observed value at the moment t; λ is the attenuation weight, $0 < \lambda < 1$.

Figure 21

Exponential Weighted Moving Average Changes Before and After Qi

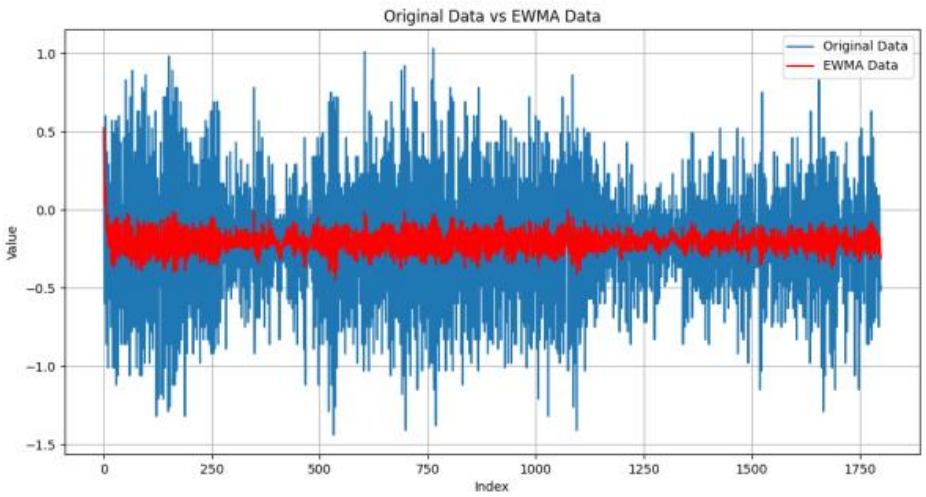

As can be seen from Figure 21, the changes in the processed data tend to be stable, the noise is reduced, and the correlation is enhanced in the long term, which can effectively avoid data jitter.

Selection of Test Platform and Fusion Algorithm

Data collection was carried out separately using STM32 and FPGA systems, and the collected signals were subsequently fused. At the same time, D-S evidence theory has a good ability to solve random uncertainty and fuzzy uncertainty, can reduce the hypothesis set by relying on cumulative evidence (F. et al., 2024), and does not require a prophetic probability function. Therefore, D-S evidence theory was chosen for the study of data fusion. Compared to Kalman and particle filters, D-S evidence theory offers distinct advantages when handling uncertain and conflicting sensor outputs. In real-world industrial settings with environmental noise and sensor inconsistencies, the ability of D-S theory to integrate multiple pieces of evidence without requiring a predefined probabilistic model makes it especially valuable. Additionally, its flexibility in accommodating partial knowledge and degrees of ignorance enables it to produce more reliable fusion outcomes when sensor reliability dynamically fluctuates.

Experimental Results

Figure 22

Comparison Before and After STM32 Acquisition Data

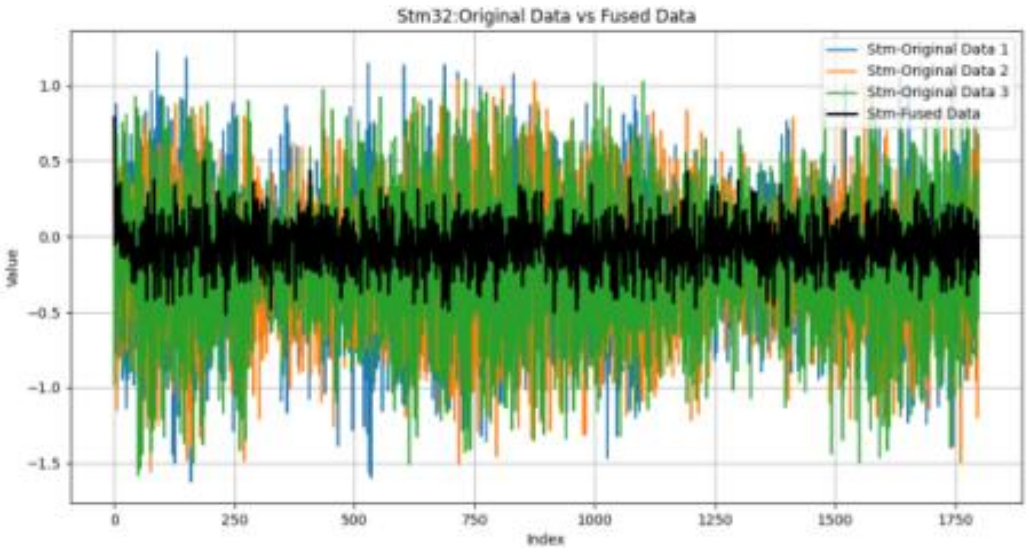

Figure 23

Comparison Before and After FPGA Acquisition Data Fusion

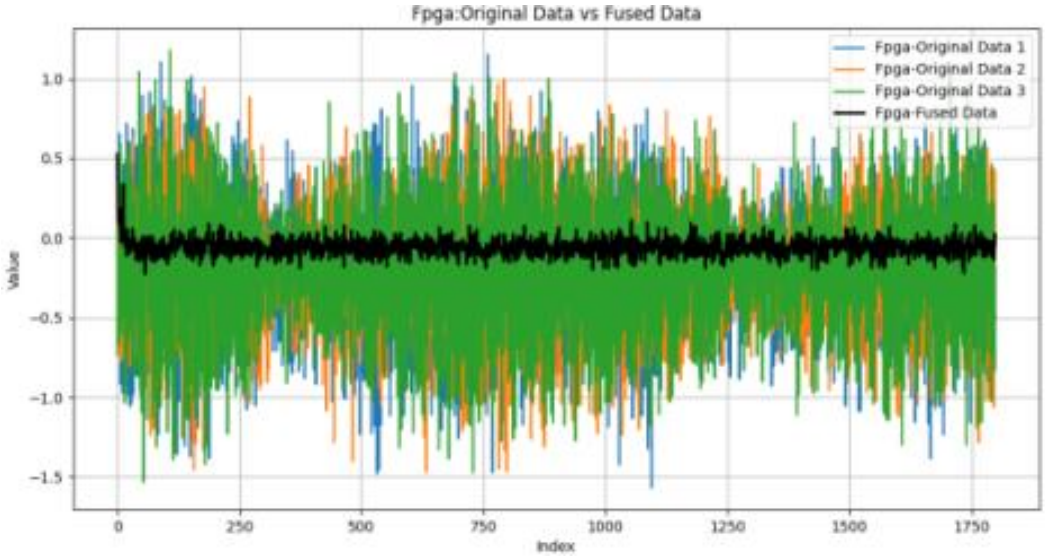

In Figure 22 and Figure 23 above, green, orange, and blue are the original data curves tested by the three vibration acceleration sensors respectively. The black curve is the data after fusion by D-S evidence theory. It can be found that the fusion effect is more obvious.

The MSE calculation was performed on the data before and after data fusion, and the data was tested using the Siemens test system. The results were summarized by Table 2.

Table 2 MSE

Result Values Before and After Data Fusion

	Sensor-1	Sensor-2	Sensor-3	D-S
STM32-MSE	0.25412	0.23092	0.26579	0.02285
FPGA-MSE	0.22582	0.20533	0.23884	0.00252

As can be seen from Table 2, the MSE values of the signals after using D-S evidence theory fusion are smaller than the MSE values of single sensor signals; the data collected using FPGA is more accurate than the data collected by STM32 and is different from the data collected by the Siemens system, although small. Experiments show that the system built using FPGA has higher accuracy, and the D-S evidence theory can effectively fuse data.

Discussion

Despite the effectiveness of the proposed system, two limitations still exist. The first area that can be improved is selection of vibration sensors. Our approach to choosing vibration sensors was somewhat rough, which might have affected the accuracy and reliability of the collected data. Specifically, while the ADXL345 accelerometer used is known for its high precision and low power consumption, our

criteria for sensor placement and selection could have been more stringent. To enhance future research, we should consider a more detailed analysis of the specific characteristics required for the sensors in the context of the machine tool's operating environment. Additionally, exploring sensors with better synchronization capabilities and lower susceptibility to external interferences could lead to more accurate data acquisition and ultimately more reliable results from the data fusion process. Moreover, another area that could be improved in the application of D-S evidence theory in the paper is its handling of conflicting evidence. The current synthesis rules of D-S evidence theory can result in high levels of conflict when combining multiple pieces of evidence, particularly if they are highly contradictory. This can lead to unreliable or misleading fusion results. To address this, implementing conflict resolution strategies, such as weighted combination approaches or the use of alternative evidence combination rules, could enhance the robustness and reliability of the data fusion process. Additionally, exploring advanced normalization techniques to better manage the influence of conflicting evidence could further improve the accuracy and applicability of D-S evidence theory in multi-sensor data fusion scenarios.

Conclusion

This study successfully addressed the research question by designing and validating a high-precision, high-synchronization data acquisition system based on the FPGA chip EP4CE6E22C8N, and by applying Dempster–Shafer (D-S) evidence theory to fuse vibration signals collected from multiple sensors. Experimental results

demonstrated that multi-sensor vibration acceleration data, when processed through the D-S evidence fusion algorithm, led to significantly enhanced measurement accuracy. Notably, the fused results closely matched those obtained from the high-end Siemens vibration testing system, confirming the effectiveness of the proposed method. Compared to traditional STM32-based systems and even commercial solutions, the proposed FPGA-based platform delivered more accurate and stable measurements, as reflected by reduced mean square error (MSE) values and smoother signal curves.

Although limitations remain in sensor selection and conflict resolution within D-S theory, the research results clearly validate the efficiency of integrating FPGA-based architecture with D-S data fusion. This proposed framework offers a reliable and cost-efficient solution for improving vibration signal measurements in machine tool bearings, thus successfully and comprehensively answers the research question, laying the groundwork for future enhancements in intelligent condition monitoring and predictive maintenance systems.

References

Abdellatif, A. G., Salama, A. A., Zied, H. S., Elmahallawy, A. A., & Shawky, M. A. (2023). An improved indoor positioning based on crowd-sensing data fusion and particle filter. *Physical Communication, 61*, 102225. https://doi.org/10.1016/j.phycom.2023.102225

A. F., Seher, M., Muhammad, H., & Shahid, M. (2024). Joint monitoring of mean and variance using Max-EWMA control chart under lognormal process with application to engine oil data. *Scientific Reports, 14*(1), 13811–13811. https://doi.org/10.1038/s41598-024-64292-1

Apriyansa, A., Bintoro, J., & Sandi, E. (2021, October). Development of early real-time disaster mitigation warning system landslide with gyroscope ADXL345 sensor. In *Journal of Physics: Conference Series* (Vol. 2019, No. 1, p. 012080). IOP Publishing. https://doi.org/10.1088/1742-6596/2019/1/012080

Deng, Z., & Wang, J. (2020). Multi-sensor data fusion based on improved analytic hierarchy process. *IEEE Access*, 8, 9875–9895. https://doi.org/10.1109/access.2020.2964729

Holovatyy, A., Teslyuk, V., Iwaniec, M., & Mashevska, M. (2017). Development of a system for monitoring vibration accelerations based on the Raspberry Pi microcomputer and the ADXL345 accelerometer. *Восточно-Европейский журнал передовых технологий [Eastern-European Journal of Enterprise Technologies], 6*(9), 52–62. https://doi.org/10.15587/1729-4061.2017.116082 (in Russian)

Liang, X., Luo, Y., Deng, F., & Li, Y. (2022). Application of improved MFDFA and DS evidence theory in fault diagnosis. *Applied Sciences, 12*(10), 4976. https://doi.org/10.3390/app12104976

Liao, M., Nie, G., Zhao, J., & He, X. (2023). Design of a baseband signal for the 406 MHz satellite emergency radio transmitter based on STM32. *Electronics, 12*(12), 2717. https://doi.org/10.3390/electronics12122717

Shen, Y., Zhao, Z., Yuan, M., & Wang, S. (2023). Research on multi-sensor data fusion positioning method of unmanned ships based on threshold-and hierarchical-capacity particle filter. *Applied Sciences, 13*(18), 10390. https://doi.org/10.3390/app131810390

Ullah, I., Youn, J., & Han, Y. H. (2021). Multisensor data fusion based on modified belief entropy in Dempster–Shafer theory for smart environment. *IEEE Access, 9*, 37813–37822. https://doi.org/10.1109/access.2021.3063242

Wu, L., Guo, W., Tang, Y., Sun, Y., & Qin, T. (2024). Remaining useful life prediction of lithium-ion batteries based on neural network and adaptive unscented Kalman filter. *Electronics, 13*(13), 2619. https://doi.org/10.3390/electronics13132619

Zhou, M., Li, X., Wang, Y., Li, S., Ding, Y., & Nie, W. (2020). 6G multisource-information-fusion-based indoor positioning via Gaussian kernel density estimation. *IEEE Internet of Things Journal, 8*(20), 15117–15125. https://doi.org/10.1109/jiot.2020.3031639

Zhu, C., Qin, B., Xiao, F., Cao, Z., & Pandey, H. M. (2021). A fuzzy preference-based Dempster–Shafer evidence theory for decision fusion. *Information Sciences, 570,* 306–322. https://doi.org/10.1016/j.ins.2021.04.059

Zhu, Z., Lu, J., & Zhu, S. (2023). Multi-rate Kalman filtering for structural dynamic response reconstruction by fusing multi-type sensor data with different sampling frequencies. *Engineering Structures, 293*, 116573. https://doi.org/10.1016/j.engstruct.2023.116573

Appendix -- Timeline and Plan

1. 2024.3.20 – 2024.6.10 | System Design and Preparation

·Completed literature review on vibration measurement and multi-sensor data fusion methods.

·Selected ADXL345 accelerometers and designed the STM32-based data acquisition system.

·Assembled initial experimental platform on the VM1050S CNC machine tool.

·Built and tested the STM32 prototype circuit board.

2. 2024.6.10 – 2024.7.10 | STM32 Preliminary Data Collection

·Collected initial vibration data using 3 ADXL345 sensors installed around the x-axis bearing.

·Applied exponentially weighted moving average (EWMA) for data smoothing.

·Observed significant sensor signal variation and timing issues.

3. 2024.7.10 | First Draft of Research Paper Completed

·Completed the first full draft of the research paper summarizing initial design, data collection, and preliminary results.

·Identified major technical gaps and opportunities for improvement during writing.

4. 2024.8.1 – 2024.10.15 | FPGA System Development and Testing

·Designed and built an FPGA-based data acquisition system using Cyclone IV FPGA.

·Repeated vibration data collection experiments with improved synchronization and higher sampling rate.

·Verified significant reduction in sensor reading discrepancies.

5. 2024.10.16 – 2024.12.15 | Fusion Algorithm Testing and Selection

·Implemented and compared Kalman filtering, particle filtering, and D-S evidence theory.

·Selected D-S evidence theory as the most effective method for managing sensor uncertainty and fusing data.

6. 2025.1.5 – 2025.2.20 | Final Experiments and Validation

·Conducted final data collection using the FPGA system.

·Applied D-S evidence theory to fuse multi-sensor data.

·Benchmarked results against Siemens professional testing system, achieving comparable measurement accuracy.

7. 2025.2.21 – 2025.3.25 | Paper Revision and Refinement

·Updated the research paper to incorporate new FPGA and fusion experiment results.

·Strengthened analysis of experimental outcomes and discussed limitations.

8. 2025.3.26 – 2025.4.10 | Final Reflection and Future Work

·Reflected on sensor selection and conflict resolution challenges.